

## **ELECTRONIC SUPPLEMENTARY INFORMATION FOR:**

Plasmonic and label-free real-time quantitative PCR for point-of-care diagnostics

Padideh Mohammadyousef,<sup>1</sup> Miltiadis Paliouras,<sup>2, 3§</sup> Mark A. Trifiro,<sup>2, 3</sup> and Andrew G. Kirk<sup>1§</sup>

<sup>1</sup>Department of Electrical and Computer Engineering, McGill University, Montreal, QC, Canada

<sup>2</sup>Lady Davis Institute for Medical Research - Jewish General Hospital, Montreal, QC,  
Canada

<sup>3</sup>Department of Medicine, McGill University, Montreal, QC, Canada

### **§Corresponding authors:**

Miltiadis Paliouras, Ph.D.

Assistant Professor

McGill University

Lady Davis Institute for Medical Research – Jewish General Hospital

Montreal, QC H3T 1E2, Canada

miltiadis.paliouras@mcgill.ca

Andrew G. Kirk, Ph.D.

Professor

Department of Electrical and Computer Engineering

McGill University

Montreal, QC H3A 0E9, Canada

andrew.kirk@mcgill.ca

## **Supplemental Material**

**S1. Positive and negative PCR protocols used for plasmonic *Chlamydia Trachomatis* DNA amplification.**

**S2. Positive plasmonic PCR protocol with increasing AuNRs concentrations.**

**S3. Zemax optical model to maximize VCSEL-to-tube coupling efficiency.**

**S4. COMSOL model geometry for time-dependent cooling of 20  $\mu$ L water inside PCR tube.**

**S5. UV-vis spectra of positive PCR samples before and after PCR with different polymerases.**

**S6. TEM images of AuNRs suspended in PCR reaction.**

**S7. Zemax optical model for the real-time UV detection system.**

**S8. Fitting algorithm used for UV transmission curves**

**S9. Unnormalized UV optical power detected at photodetector for positive and negative PCR controls.**

**S10. Repeatability of PCR results determination based on UV curves.**

**S11. Normalized UV curves obtained from plasmonic thermocycling of each PCR ingredient separately.**

**S12. Comparison of UV system and qPCR limit of detection**

**S13. UV transmission spectrum of the plastic PCR tube and the emission spectrum of the UV LED.**

## S1. Positive and negative PCR protocols used for plasmonic *Chlamydia Trachomatis* DNA amplification.

**Table 1** Positive PCR protocol for KlenTaq polymerase.

PCR component	Volume ( $\mu\text{L}$ )
5X Taq Reaction Buffer	4
Taq polymerase	0.8
dNTP (2 mM)	0.6
Forward Primer (5 $\mu\text{M}$ )	0.6
Reverse Primer (5 $\mu\text{M}$ )	0.6
DNA ( $10^4$ copies)	1
PEG-AuNRs (50 nM)	1
ddH <sub>2</sub> O	11.4
Total	20

**Table 2** Positive PCR protocol for Kapa2G polymerase.

PCR component	Volume ( $\mu\text{L}$ )
Kapa2G Reaction Buffer	4
Kapa2G polymerase	0.1
dNTP (2 mM)	0.6
Forward Primer (5 $\mu\text{M}$ )	1
Reverse Primer (5 $\mu\text{M}$ )	1
DNA ( $10^4$ copies)	1
PEG-AuNRs (50 nM)	1
ddH <sub>2</sub> O	11.3
Total	20

**Table 3** Positive PCR protocol for Phusion polymerase.

PCR component	Volume ( $\mu\text{L}$ )
Phusion Reaction Buffer	4
Phusion polymerase	1
dNTP (2 mM)	0.6
Forward Primer (5 $\mu\text{M}$ )	1
Reverse Primer (5 $\mu\text{M}$ )	1
DNA ( $10^4$ copies)	1
PEG-AuNRs (50 nM)	1
ddH <sub>2</sub> O	10.4
Total	20

**Table 4** Negative Controls with KlenTaq polymerase.

PCR component	Volume ( $\mu\text{L}$ )		
	No DNA	No Polymerase	No Forward Primer
5X Taq Reaction Buffer	4	4	4
Taq polymerase	0.8	0	0.8
dNTP (2 mM)	0.6	0.6	0.6
Forward Primer (5 $\mu\text{M}$ )	0.6	0.6	0
Reverse Primer (5 $\mu\text{M}$ )	0.6	0.6	0.6
DNA ( $10^4$ copies)	0	1	1
PEG-AuNRs (50 nM)	1	1	1
$\text{d}_2\text{H}_2\text{O}$	12.4	12.2	12
Total	20	20	20

**S2. Positive plasmonic PCR protocol with increasing AuNRs concentrations.****Table 5** Positive PCR protocol with KlenTaq polymerase for 2.5-29 nM AuNRs concentration.

AuNRs Final Concentration (nM)	PEG-AuNRs stock solution ( $\mu\text{L}$ )	ddH <sub>2</sub> O ( $\mu\text{L}$ )	Rest of PCR reagents ( $\mu\text{L}$ )
2.5	1	11.4	7.6
4	1.6	10.8	
6	2.4	10	
8	3.2	9.2	
10	4	8.4	
12	4.8	7.6	
15	6	6.4	
20	8	4.4	
29	11.6	0.8	

### S3. Zemax optical model to maximize VCSEL-to-tube coupling efficiency.

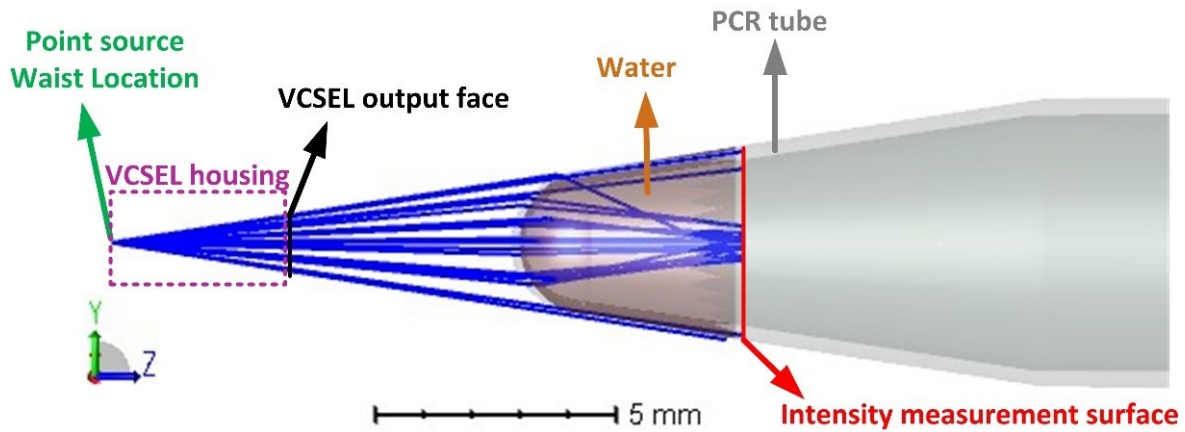


Fig. 1 Zemax non-sequential model for the VCSEL-based plasmonic thermocycler to maximize coupling efficiency.

### S4. COMSOL model geometry for time-dependent cooling of 20 $\mu\text{L}$ water inside PCR tube.

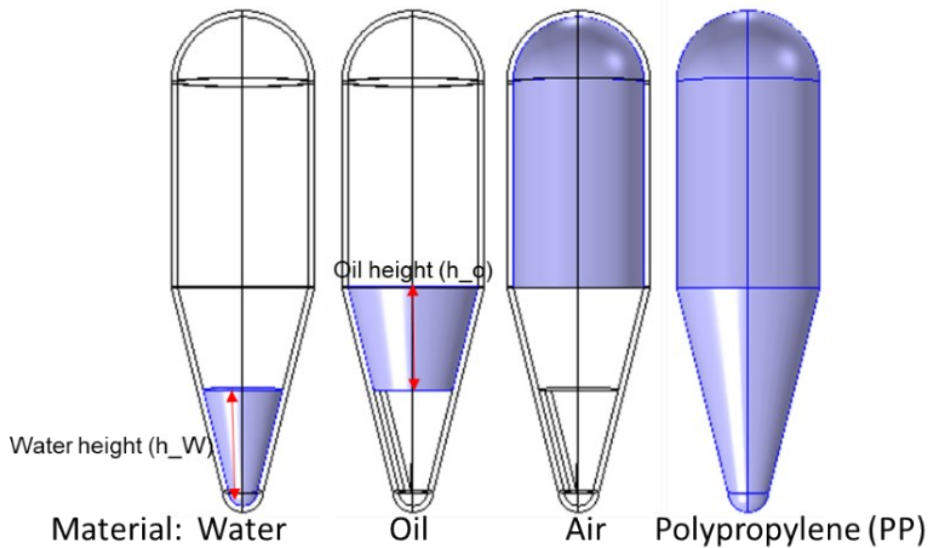
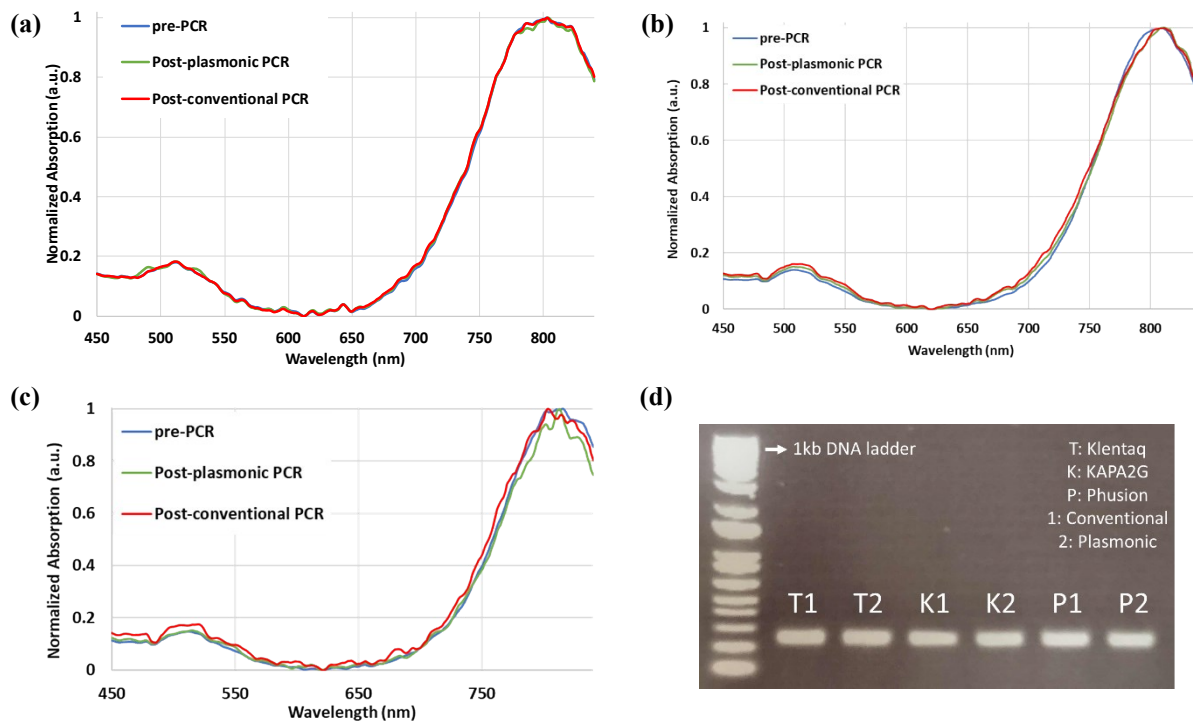


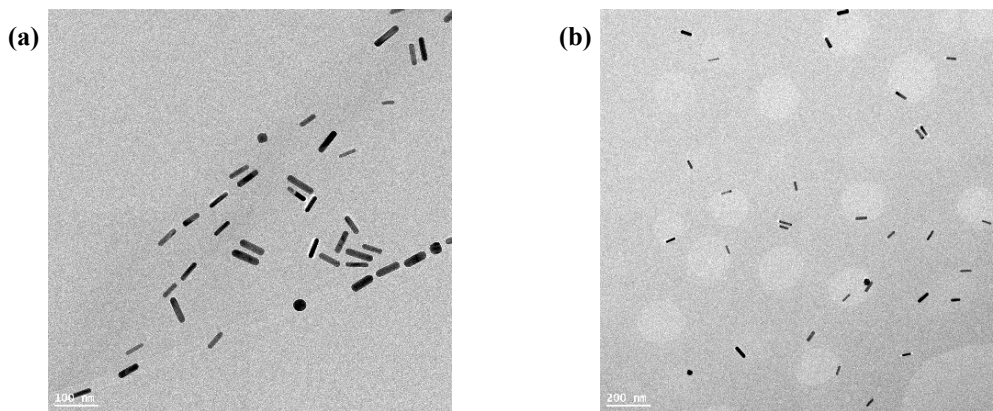
Fig. 2 COMSOL model geometry description.

## S5. UV-vis spectra of positive PCR samples before and after PCR with different polymerases.



**Fig. 3** Min-max normalized absorption spectra of PCR samples before and after PCR with (a) KlenTaq, (b) Kapa2G, and (c) Phusion polymerases underwent both conventional and plasmonic amplification. It is evident that AuNRs' absorption property remains intact after plasmonic and conventional amplification. (d) Gel electrophoresis image of post-PCR samples retrieved from plasmonic and conventional thermocyclers.

## S6. TEM images of AuNRs suspended in PCR reaction.



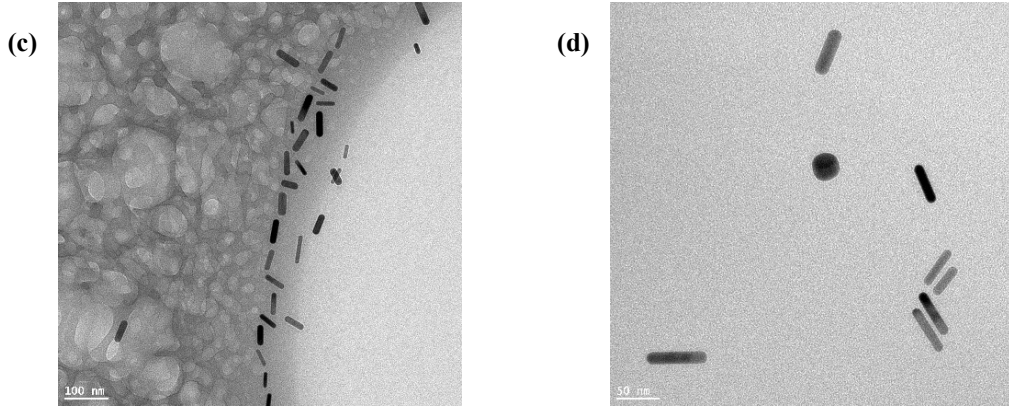


**Fig. 4** TEM images for (a) Pre-PCR positive, (b) Post-PCR positive (c) Pre-PCR negative and (d) Post-PCR negative controls.

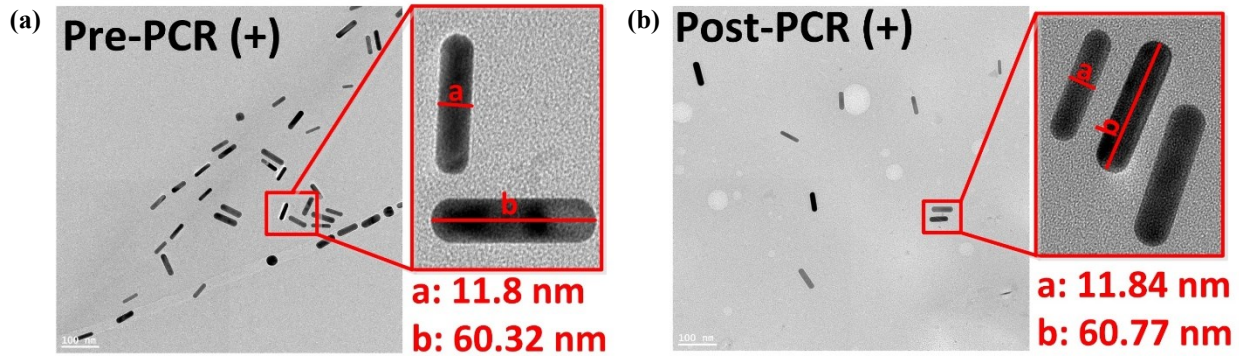


**Fig. 5** Close up TEM images captured from AuNRs from (a) pre-PCR and (b) post-PCR samples demonstrating unaltered AuNRs size and morphology.

## S7. Zemax optical model for the real-time UV detection system.

To maximize UV optical power at photodetector ( $P_{\text{detector}}$ ), we performed a radiometric analysis in Zemax optical design software in non-sequential mode. The UV LED was modeled as a source radial with 1 mW output optical power ( $P_{\text{source}}$ ), 260 nm nominal wavelength, 3 mm  $\times$  3 mm flat rectangular emitting region, and symmetric distribution of rays into a hemisphere. The far-field intensity distribution of Thorlabs UV LED, provided in its datasheet, was used to define the relative intensity measured in the far-field of the source radial at specific angles. Next, we modeled Thorlabs photodetector with a flat absorbing rectangular detector (2.2 mm  $\times$  2.2 mm) to store the energy data from non-sequential source rays that strike it. The model geometry is such that the

optical axis is perpendicular to the cone axis of the PCR tube (Fig. 6.a), and the material selected for tube and PCR reaction were polypropylene and water, respectively. Owing to optical system assembly limitations in practice such as the thickness of optical cage system mounting plates and the thickness of PCR tube holder, the shortest distance to place UV LED and photodetector with respect to PCR tube is 9 mm, and thereby the same distances were considered in the optical model. Furthermore, we considered that the non-sequential rays from source radial were statistically scattered at ray-surface intercepts. Fig. 6.b displays the rectangular detector view together with spatially incoherent irradiance at the detector. In this figure, the total power indicates that 9.83%

of source radial optical power reaches at detector ( $\frac{P_{\text{detector}}}{P_{\text{source}}} = 0.098$ ) with this optical setup. To

enhance  $\frac{P_{\text{detector}}}{P_{\text{source}}}$ , two converging lenses were used, and their characteristics were optimized in the non-sequential mode for maximum optical power at the detector. We found that UV-AR coated double-convex (DCX) lens (EFL: 6 mm and  $f/\#$ : 1) from Edmund Optics were the best fit for the optimized converging lenses data. Therefore, the first DCX lens was placed between UV LED and PCR tube, and the second lens was placed between tube and photodetector (Fig. 6.c). The center-to-center separation distance between each lens and PCR tube is 9 mm. Using this optical setup,

the  $\frac{P_{\text{detector}}}{P_{\text{source}}}$  is 0.127 with an approximately 30% increase in comparison with the no-lens setup (Fig. 6.d). Thus, we used the 2-lens system for our real-time plasmonic PCR product detection.

**(a)**

**(b)**

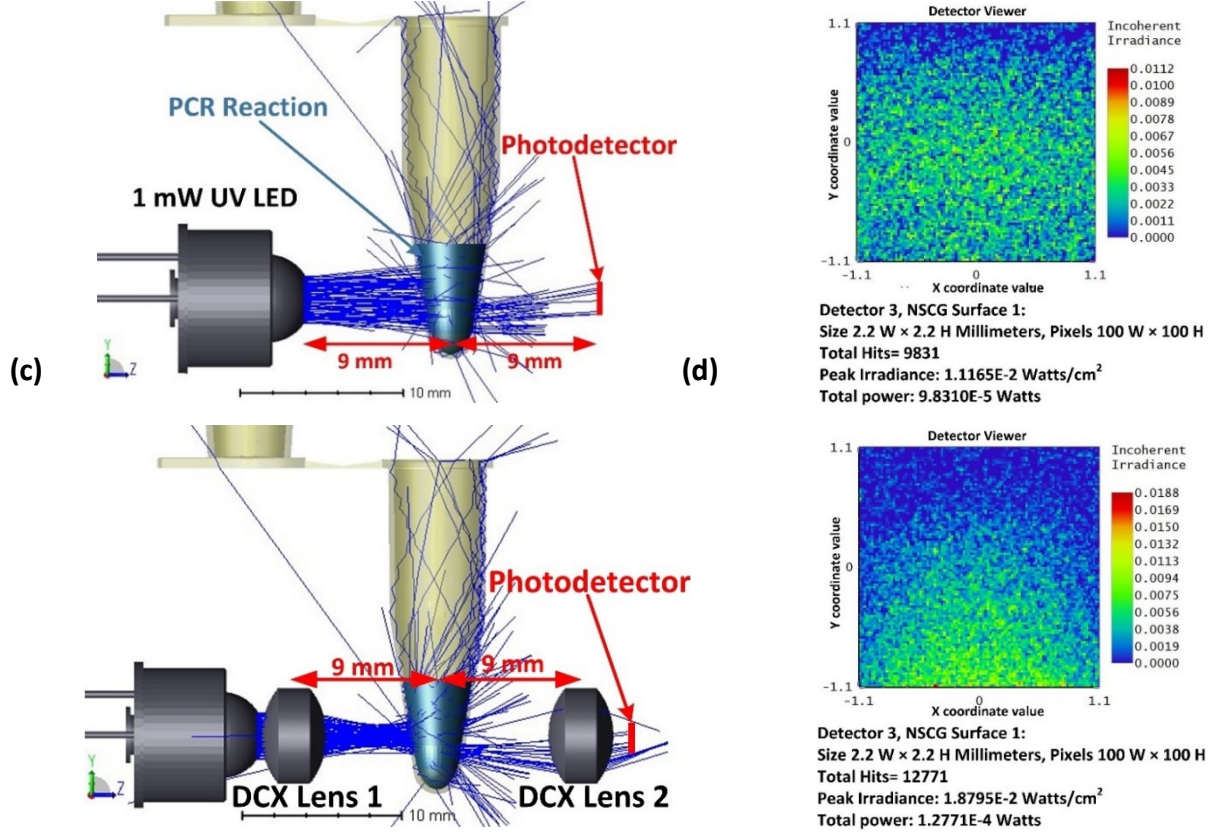


**Fig. 6** Optical simulation for the UV detection system. Optical configurations and ray-tracing diagrams for (a) no-lens system and (c) 2-lens system. Detector viewer for (b) no-lens and (d) 2-lens UV detection system.

### S8. Fitting algorithm used for UV transmission curves

UV transmission data points were divided into two PCR cycle subsets of  $[1, m]$  and  $[m+1, 40]$  where  $m$  is a cycle number between 1 and 40. An exponential ( $f_{exp,m}$ ) and a sigmoid curve ( $f_{sigmoid,m}$ ) were least-square fitted to the  $[1, m]$  and  $[m+1, 40]$  subsets, respectively. The least-square error between the fitted curves and data points are as follows:

$$E(f_{exp,m}) = \left( \frac{1}{m} \sum_{x=1}^m (f_{exp,m}(x) - P_x)^2 \right)^{\frac{1}{2}} \quad (1)$$

$$E(f_{sigmoid,m}) = \left( \frac{1}{40-m} \sum_{x=m+1}^{40} (f_{sigmoid,m}(x) - P_x)^2 \right)^{\frac{1}{2}} \quad (2)$$

$$E(f_{UV\ curve,m}) = E(f_{exp,m}) + E(f_{sigmoid,m}) \quad (3)$$

Where  $E$  is the least-square error,  $x$  is the cycle number,  $f_{exp,m}$  is the fitted exponential curve,  $f_{sigmoid,m}$  is the fitted sigmoid curve, and  $P_x$  is the experimental UV transmission data point. The cycle number ( $m$ ) which gives the minimum  $E(f_{UV\ curve,m})$  is selected as the threshold cycle ( $C_t$ ), and the  $f_{exp,C_t}$  and  $f_{sigmoid,C_t}$  are the best fitted curves to the UV transmission data points.

$$E(f_{UV\ curve,C_t}) = \min(E(f_{UV\ curve,m})), \quad 1 \leq m \leq 40 \quad (4)$$

### S9. Unnormalized UV optical power detected at photodetector for positive and negative PCR controls.

It is important not to compare UV transmitted optical power values of one experiment to another since UV transmission varies even for the same PCR solution pipetted in different PCR tubes or the same PCR tube with a change of its side facing the UV LED. This is due to changes occurring in pipetting, optical alignment for each experiment, or differences in shape and wall thickness of each side of the PCR tube. This implies that for a valid comparison between two different experiments, only UV transmission behavior throughout 40 cycles should be considered. Thus, UV amplification curves were min-max normalized to clearly compare their behavior/shape and extract distinctive features for positive/successful and negative/failed PCR differentiation.

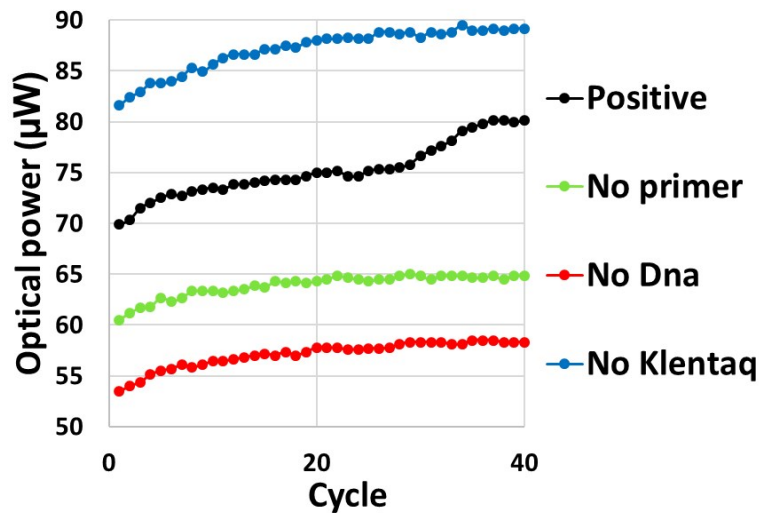


Fig. 7 UV transmission at photodetector for different controls.

The functions least-square fitted to UV data are as follows:

$$P_{Positive} = \begin{cases} b_1 e^{a_1 x} + b_2 e^{a_2 x} & 1 \leq x \leq C_t \\ \frac{b_3}{1 + e^{a_3 x + c_1}} & C_t \leq x \leq 40 \end{cases} \quad (5)$$

$$P_{Negative} = b_4 e^{a_4 x} + b_5 e^{a_5 x} \quad (6)$$

Where  $x$  is cycle number and  $C_t$  is the threshold cycle equal to 27 in this experiment (Fig. 7). The coefficients in eqn 1 and eqn 2 were quantified for normalized UV curves presented in Fig. 9A in the main manuscript.

**Table 6** Quantified coefficients for  $P_{Positive}$

$a_1$	$a_2$	$a_3$	$b_1$	$b_2$	$b_3$	$c_1$
0.02	-0.3	-0.2	0.3	-0.4	1.1	5.6

**Table 7** Quantified coefficients for  $P_{Negative}$

	$a_4$	$a_5$	$b_4$	$b_5$
No primer	-4e-3	-0.09	1.14	-1.2
No DNA	9e-3	-0.15	0.54	-0.6
No Taq	-2e-3	-0.07	1.14	-1.2

### S10. Repeatability of PCR results determination based on UV curves.

To demonstrate the repeatability of our method, we randomly collected UV curves obtained from real-time plasmonic amplification of 20 different PCR samples. These samples were prepared from different master mix solutions and went through plasmonic amplification on different days. The initial DNA copy numbers of samples are either  $10^4$  or  $10^5$ . The samples were positive PCR controls following the KlenTaq polymerase PCR protocol (Table 1). Next, we classified the UV curves obtained from these 20 PCR reactions into two categories of “success” and “fail” based on

their results on gel image. Then,  $P_{40}/P_{C_t}$  and  $P_{C_t}/P_1$  were calculated for both categories and plotted in Fig. 8. It should be noted that in this section, the failed PCRs were not negative PCR controls, but rather positive controls which underwent various PCR conditions leading to PCR inhibition or

failed PCR. The results in Fig. 8 shows that for all successful PCR experiments,  $\frac{P_{C_t}^2}{P_{40} \times P_1}$  is less than 1.15 indicating the validity and repeatability of our method.

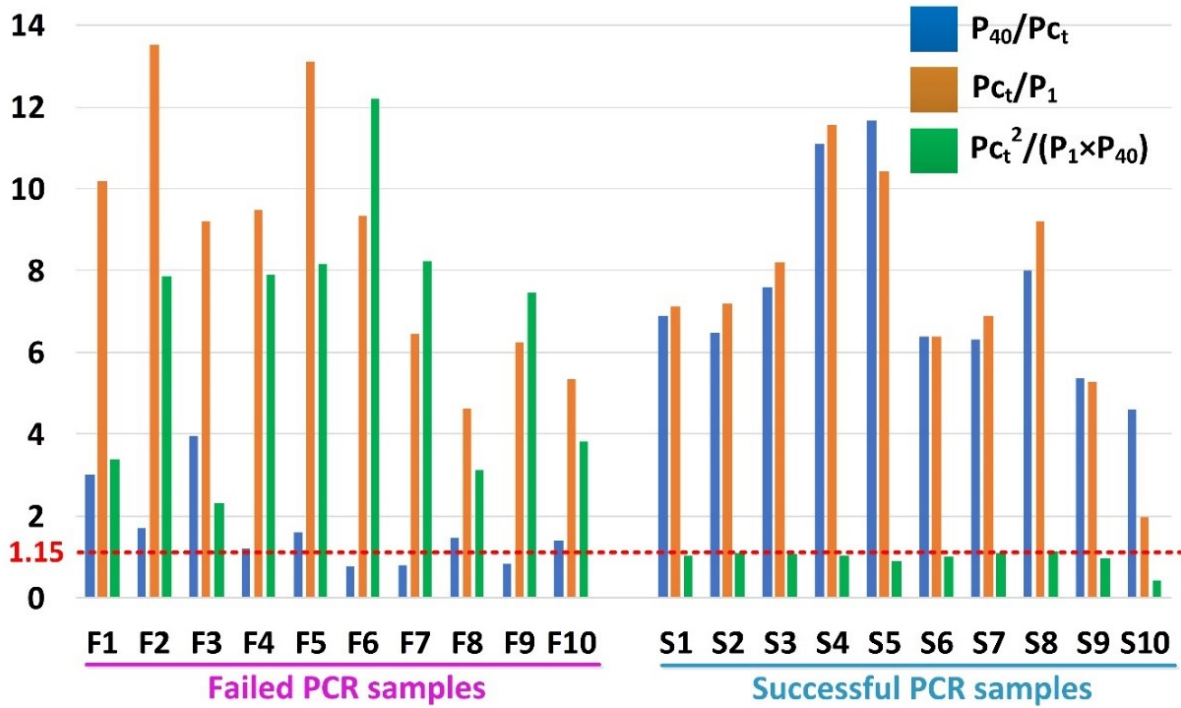


**Fig. 8** The rectangular blue and orange bars represent calculated  $P_{40}/P_{C_t}$  and  $P_{C_t}/P_1$  for 20 different plasmonic positive PCR samples. The first 10 samples are failed PCR tests with  $\frac{P_{C_t}^2}{P_{40} \times P_1}$  (green bars) greater than 1.15, whereas  $\frac{P_{C_t}^2}{P_{40} \times P_1}$  is less than or equal to 1.15 for successful PCR tests.

**S11. Normalized UV curves obtained from plasmonic thermocycling of each PCR ingredient separately.**

We compared real-time UV curves generated from plasmonic thermocycling of each PCR ingredient separately. AuNRs and each ingredient were diluted with ddH<sub>2</sub>O to obtain 20 μL sample volume. The final concentration of reagents is the same as in positive PCR.

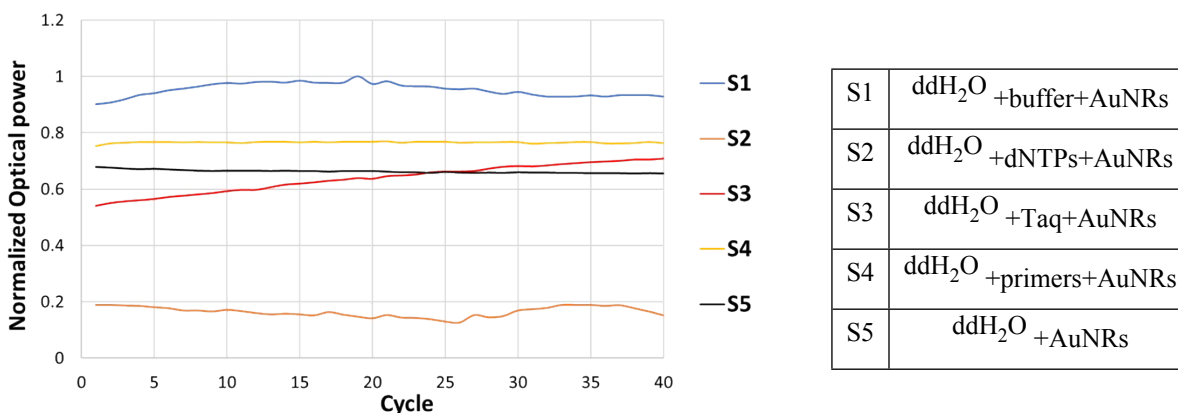


**Fig. 9** Min-max normalized UV optical power from plasmonic thermocycling of each PCR ingredient separately. Only the sample with KlenTaq polymerase (S3, red) showed increasing UV transmission throughout 40 cycles.

## S12. Comparison of UV system and qPCR limit of detection

We attempted to compare the detection sensitivity of fluorescent PCR (qPCR) with the UV monitoring system. To fulfill this, qPCR experiments were carried out in Applied Biosystems 7500 fast real-time PCR system using a ready-made qPCR kit which provides a blend of polymerase, buffer, and dNTPs. The default setting on the qPCR machine has the minimum denaturing, annealing, and elongation hold-times of 30 s, i.e., shorter time intervals are not allowed to be performed on the qPCR software. In contrast to the qPCR system, UV monitoring detection provides the flexibility of altering the polymerase type, PCR reagents concentrations, and hold-times. Therefore, accurate comparing of UV detection sensitivity with qPCR is a challenge due to different types of PCR components and their concentrations as well as their PCR running conditions. To assess the detection sensitivity of qPCR, different samples containing varying DNA template concentrations of *C. Trachomatis* DNA were diluted with the qPCR master mix/qPCR kit purchased from QIAGEN, and they underwent conventional amplification in the qPCR machine. The threshold cycles of qPCR amplification curves ( $C_{t,qPCR}$ ) are compared with the

threshold cycles obtained from UV monitoring ( $C_{tUV}$ ) of samples with different initial DNA concentrations (Fig. 10).

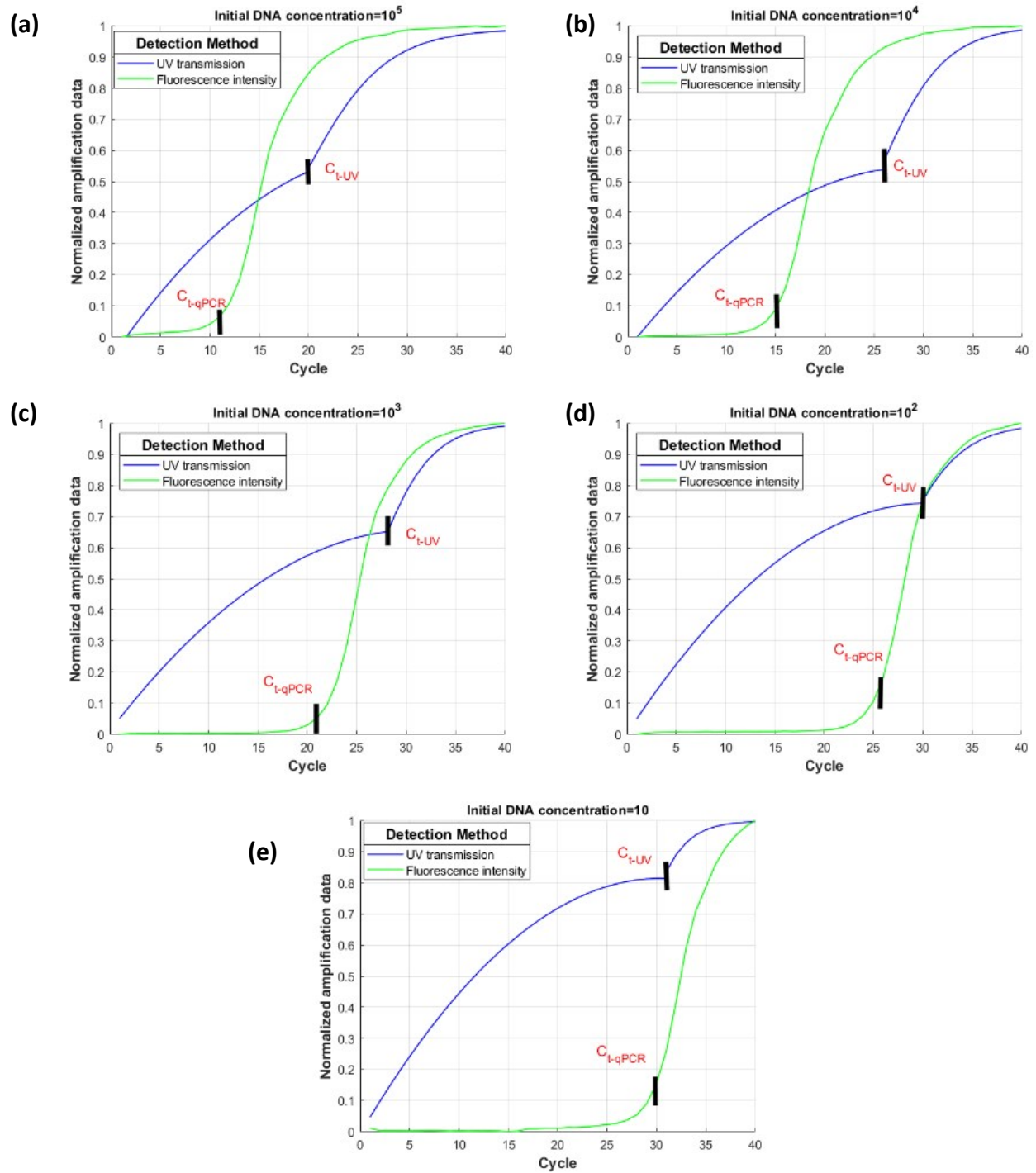


**Fig. 10** Comparison of normalized UV and fluorescent amplification curves using (a)  $10^5$ , (b)  $10^4$ , (c)  $10^3$ , (d)  $10^2$ , and (e) 10 initial DNA copy numbers.

### S13. UV transmission spectrum of the plastic PCR tube and the emission spectrum of the UV LED.

The emission spectrum of the UV LED is obtained from Thorlabs' LED260J Optan® UV LED datasheet. Fig. 11 shows that the emission intensity spectrum depends on the operating current and temperature.

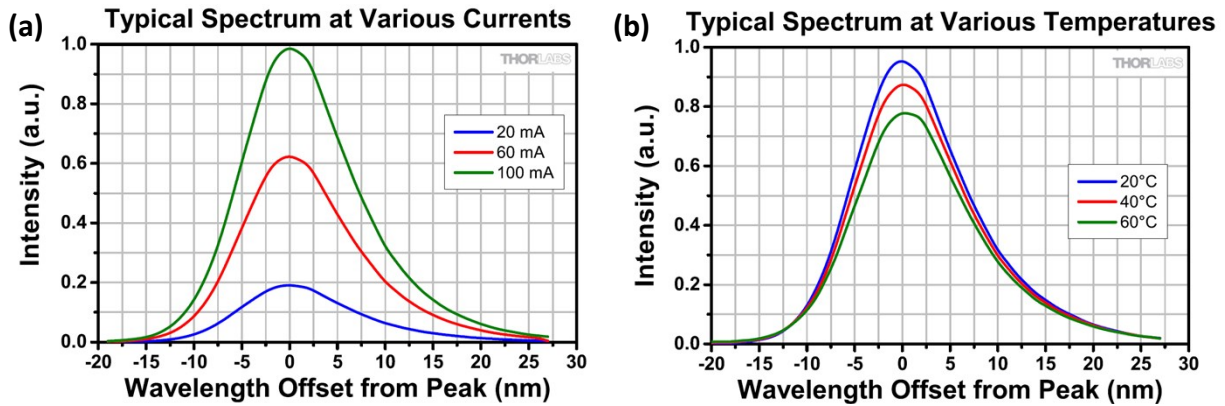


**Fig. 11** (a) UV LED emission spectra at different operating (a) currents and (b) temperatures. The intensity spectra at different temperatures were measured at 100 mA current.

In our study, the LED was driven at 100 mA at a case temperature of 25 °C. Therefore, based on the datasheet, the peak wavelength is  $260 \pm 5$  nm, FWHM bandwidth (BW) is 12 nm, and the UV LED emission spectral BW ( $BW_{UV}$ ) ranges approximately from 235 nm to 285 nm.

The conventional PCR plastic tube is made of polypropylene (PP). Fig. 12 shows the transmission spectrum and extinction coefficient for 0.5 mm-thick PP (García-Gil, Pablos et al. 2020).

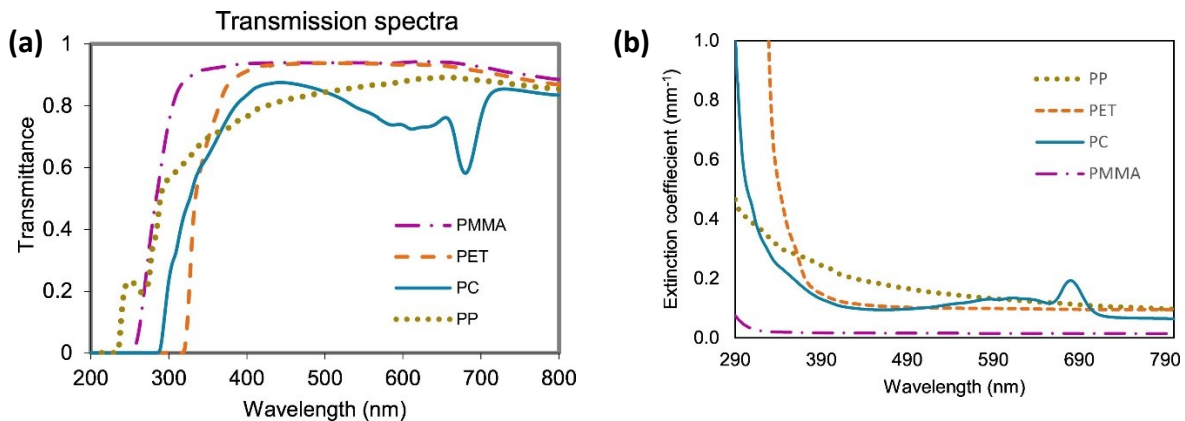


**Fig. 12** (a) Transmission spectrum and (b) extinction coefficient ( $\text{mm}^{-1}$ ) for 0.5 mm-thick PP (García-Gil, Pablos et al. 2020).

Since the extinction coefficient for wavelength between 235 nm and 290 nm is not given in Fig. 12.b, Beer Lambert's law (eqn (7)) and the UV transmission spectrum in Fig. 12.a were used to derive the extinction coefficient ( $\epsilon_{pp}(\lambda)$ ) of PP within  $BW_{UV}$ .

$$T = 10^{-\epsilon_{pp}(\lambda) \times th} \quad (7)$$

Where T is the light transmission,  $\epsilon_{pp}(\lambda)$  is the extinction coefficient of PP ( $mm^{-1}$ ), and  $th$  is the optical pathlength for light transmission, i.e., thickness of PP (mm).

Using the calculated  $\epsilon_{pp}(\lambda)$ , the transmission spectra of PP with varying thicknesses are calculated and plotted in Fig. 13. For PCR plastic tube, since light propagates through two PP walls with thicknesses of 0.25 mm, the transmission spectrum for  $th=0.5$  mm should be considered.

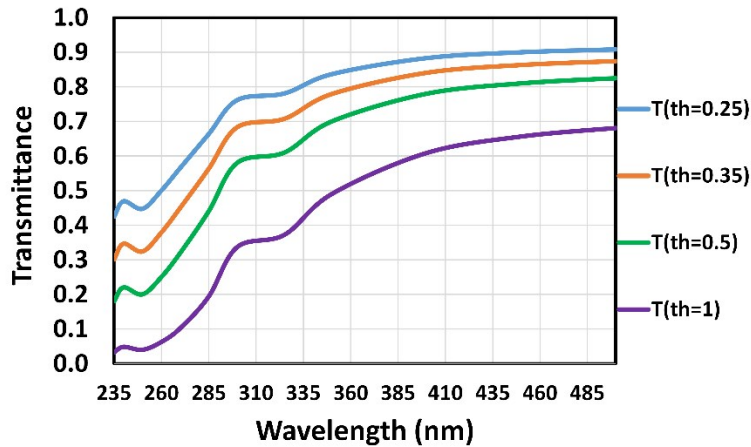


Fig. 13 Transmission spectra for PP with various thicknesses.